Commun. Comput. Phys.
doi: 10.4208/cicp.2009.09.048

Vol. 7, No. 3, pp. 580-596
March 2010

Theoretical Simulation on a Nonlinear Photonics Process of Er(1%)Yb(8%):FOV Oxyfluoride Nanophase Vitroceramics

Ce Wang[1,2], Xiaobo Chen[1,*], Gregory J. Salamo[3], Naruhito Sawanobori[4], Chenjuan He[1,2], Hongyu Zhou[1,2], Hongmei Jing[1,2], Yongzhi Zeng[5], Song Li[1,2] and Xiaoling Xu[1]

[1] *Applied Optics Beijing Area Major Laboratory, Beijing Normal University, Beijing, 100875, China.*
[2] *Applied Optics Beijing Area Major Laboratory, Department of Physics & Material College, Beijing Normal University, Beijing, 100875, China.*
[3] *Department of Physics, University Arkansas, Fayetteville, AR 72701, USA.*
[4] *Sumita Optical Glass, Inc., 4-7-25 Harigaya, Urawa, Saitama, 338, Japan.*
[5] *Department of Physics, Fuzhou University, Fuzhou, Fujian, 350002, China.*

Received 7 March 2009; Accepted (in revised version) 12 August 2009

Communicated by Haiqing Lin

Available online 8 October 2009

Abstract. We numerically simulate a photonics phenomenon of what we call intensity inversion between red and green fluorescence in oxyfluoride nanophase vitroceramics Er(1%)Yb(8%):FOV through the integration of whole fluorescence's theories. We found that it is essential to introduce a coefficient presenting the difference between the Stokes energy transfer and anti-Stokes energy transfer processes in nano-material when calculating the energy transfer rate. Under this consideration, and with the total crystallized volume ratio set to be 17.6%, the simulation results of the population probabilities values of all energy levels of Er^{3+} ion are coincident with the experimental result perfectly.

AMS subject classifications: 78A60, 37M05, 37N20, 65L07, 65Z05

Key words: Energy transfer, theoretical simulation, Stokes and anti-Stokes processes, rare earth ions, oxyfluoride nanophase vitroceramics.

1 Introduction

Energy transfer is one of the most important processes in the fluorescence of rare earth ion doped material [1]. Many phenomena that attract much interest, especially for hot

*Corresponding author. *Email address:* xbchen@bnu.edu.cn (X. Chen)

frontier nano-material, are directly related to energy transfer processes. So the determination of energy transfer rate is critical to reveal various fluorescence processes. Generally there are two methods to obtain the energy transfer rate. One is the experimental method to determine the rate using a set of materials doped with rare earth ions with different concentrations [2]. The other is the theoretical method to be discussed in the present paper. The study by Kushida in 1973 [3] has laid the foundation for this theoretical method, which led us to obtain the energy transfer rate through Judd-Oflet intensity parameters. After introducing the phonon theory by Dexter and Miyakawa [4], this method became even more practical as it allows us to solve the questions of phonon-assisted energy transfer involving energy mismatch. In fact, there are two cases of energy mismatch [5]. When the energy transferred by the donor is larger than the energy accepted by the acceptor, it is a Stokes process. On the contrary, if the transferred energy is less than the accepted energy, it is an anti-Stokes process. Usually we pay much attention on the magnitude of the energy mismatch and ignore the difference between the Stokes and anti-Stokes processes. However, in the numerical simulation on the intensity inversion phenomenon in Er(1%)Yb(8%):FOV nanophase oxyfluoride vitroceramics, we found that it is essential to consider the effects of this difference, particularly for the nano-materials where energy transfer plays a key role in the whole processes, because in the nano-scale the energy transfer rate increases greatly with the reduction in the distance between ions.

2 Experiment

The composition of Er(1%)Yb(8%):FOV is 8%YbF_3, 1%ErF_3, 30%PbF_2, 16%ZnF_2, and 45%SiO_2. The pure raw materials were put in a platinum crucible for heating at about 900°C for 100 minutes and then cooled fast at an iron plate to form oxyfluoride glass. The transparent oxyfluoride vitroceramics were obtained by annealing at the glass transition temperature for 7 hours.

The absorption spectrum was measured by using UV-365 spectrophotometer, which is shown as Fig. 1. And the fluorescence spectra were measured by using JY-ISA Fluorolog-Tau-3 fluorescence spectrophotometer. In the Stokes excitation spectra, two relatively strong excitation peaks at 378.5nm and 522.3nm, corresponding to $^4G_{11/2}$ and $^2H_{11/2}$ of Er^{3+} ion respectively, were observed. Then the Stokes emission spectra of the sample under the 0.3mw excitation at these two wavelengths were studied, as shown in Fig. 2. It can be seen that the fluorescence of $^4S_{3/2} \longrightarrow {}^4I_{15/2}$ is stronger than that of $^4F_{9/2} \longrightarrow {}^4I_{15/2}$ when the Er(1%)Yb(8%):FOV is excited by 522.3nm light, but the proportional relationship between the green and red fluorescence intensities is reversed when the sample is excited by 378.5nm light. This is the fluorescence intensity inversion phenomenon [6]. We can define the common intensity ratio α which equals to the ratio of the green fluorescence intensity I($^4S_{3/2}$) to the red one I($^4F_{9/2}$) when $^2H_{11/2}$ is excited, while the unusual intensity inversion ratio γ is equal to the ratio of I($^4F_{9/2}$) to I($^4S_{3/2}$) when $^4G_{11/2}$ is excited directly. Thus the range of intensity inversion is $\Sigma = \alpha \times \gamma$. The experimental value

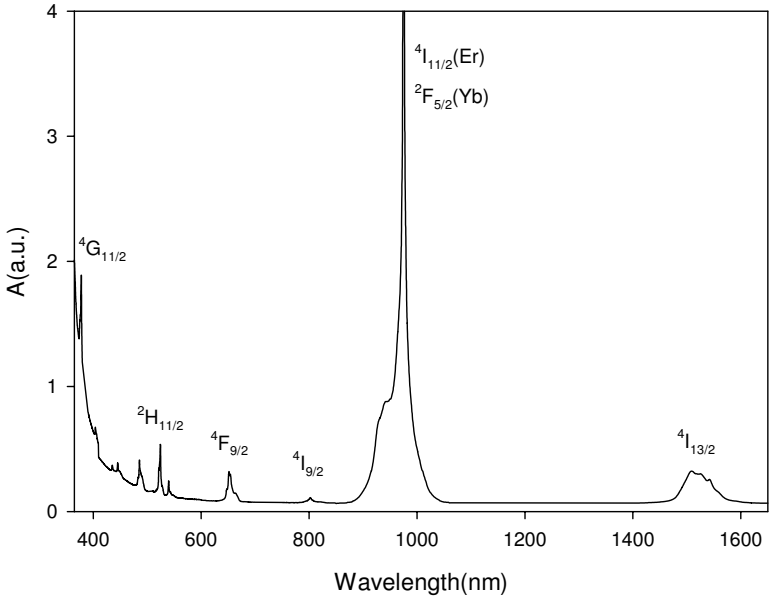

Figure 1: The absorption spectra of Er(1%)Yb(8%):FOV.

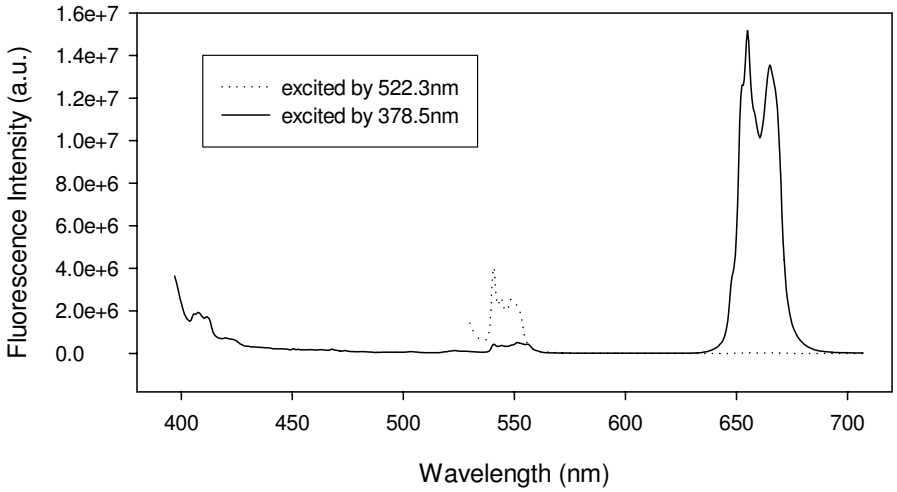

Figure 2: Emission spectra of Er(1%)Yb(8%):FOV.

of Σ for Er(1%)Yb(8%):FOV is 2701.2 due to the obvious fluorescence intensity inversion phenomenon. α is 27.39, and γ is 98.62.

The schematic of the Er^{3+} and Yb^{3+} ions' energy levels is shown in Fig. 3. The arrows represent the dominant processes in the intensity inversion phenomenon. Especially the solid lines between the Er^{3+} and Yb^{3+} ions represent the key energy transfer in this phenomenon.

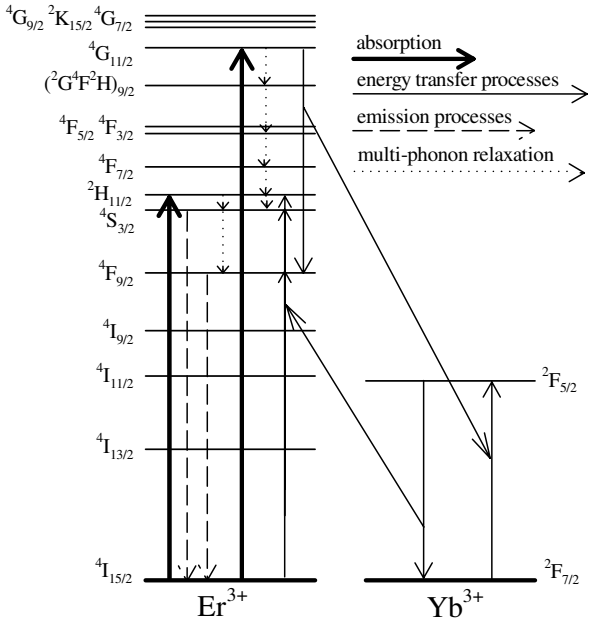

Figure 3: The schematic of the Er^{3+} and Yb^{3+} ions' energy levels.

3 The rate equations and related parameters

In this paper we focus on the numerical dynamical simulation of the intensity inversion phenomenon by solving the rate equation:

$$\frac{dn_i}{dt}=\sum_{s,p}\left\{\sum_{j,m,n,k}\left[W_s^{(j\to i)}\cdot n_j+W_p^{(m\to n,k\to i)}\cdot n_m n_k\right]-\sum_{j,m,n,k}\left[W_s^{(i\to j)}\cdot n_i+W_p^{(m\to n,i\to k)}\cdot n_m n_i\right]\right\}, \tag{3.1}$$

where n_i is the population probability of level i.

$W_s^{(j\to i)}$ denotes the transition rates of induced emission, absorption, spontaneous emission and multi-phonon relaxation, from level j to i, which can be calculated through the absorption spectra and lifetime by using Judd-Ofelt theory [7].

In the rare earth ion doped materials, the electric-dipole transition is allowed because the odd terms of the Hamiltonian of the weak crystal field make the excited configuration $4f^{n-1}n'l'$ of rare earth ion mix into the $4f^n$ to form the mixture of two configurations. So the transitions between energy states in the $4f^n$ configuration of the Er^{3+} are mostly composed of the electric-dipole transition, the magnetic-dipole transition and the electric-quadruple transition. The electric-quadruple oscillator strength is much smaller than the total oscillator strength, so we neglect its contribution. Thus the total oscillator strength equals to the sum of the electric-dipole and the magnetic-dipole oscillator strength, which can be written as $f=f_{ed}+f_{md}$. The total absorption oscillator strength from the ground

state to each excited states can be calculated from the absorption spectrum which are shown in Fig. 1.

In the J-O theory, the electric-dipole oscillator strength is expressed as a sum of the products of the optical intensity parameters Ω_t and the square of the matrix elements of the unit tensor operators $U^{(t)}$. According to J-O theory, the values of $U^{(t)}$ have little change with the ion environment, so it is usually to adopt the values reported in [8] to calculate all rare earth ion's spectroscopy.

The magnetic-dipole oscillator strength f_{md} can be computed from the magnetic dipole, by using the Winger-Eckart theory and the intermediate coupling wave functions [7]. Because the spin-orbit coupling interaction of rare earth ions is strong, we should take it together with the coulomb interaction into account when calculating the wave function of ions. The wave function should include those states which have the same value of J, but different values of L and S, that is to say, the wave function of the Er^{3+} ion in the material, which we call the intermediate coupling function, can be expressed as the linear combination of some RS states. Although ions in different environments can lead to different intermediate coupling functions, the physical quantities are not sensitive to the wave functions. So we usually use the known intermediate coupling constants to discuss the questions in different materials. The values of these constants, adopted in this paper, can be found in [9].

According to expression of total oscillator strength, the electric-dipole oscillator strength can be calculated by subtracting the magnetic-dipole oscillator strength from the total oscillator strength of the ground state absorption. Then from the measured twelve electric-dipole oscillator strengths we can fit three intensity parameters Ω_t in Er(1%)Yb(8%):FOV by using the least square method and obtain $\Omega_2 = 2.1527\times10^{-20}\text{cm}^2$, $\Omega_4 = 1.0978\times10^{-20}\text{cm}^2$, $\Omega_6 = 1.7334\times10^{-20}\text{cm}^2$.

After obtaining the values of intensity parameter Ω_t, we can calculate the oscillator strength $f_{JJ'}$ between two excited states using the J-O theory. Further according to the relation

$$A = \frac{8\pi^2 e^2 \widetilde{v}^2 n^2}{mc} f,$$

we can achieve the spontaneous emission rates. The main results are shown in Table 1.

When the pumping light is incident at the material, there are absorption transitions and induced emission transitions to be generated in the rare earth ion. The rates of these induced transitions can be expressed by absorption cross section and emission cross section. When the line broadening of the pumping light is much smaller than the spectra line broadening of the activator ion, this relationship is $R = \sigma(v)I/hv$, where R is the transition rate, I is the light intensity that equals to P/s, P is the light power and s is the area of light spot, $\sigma(v)$ is the absorption cross section or emission cross section at the wavelength of pumping. In the sample Er(1%)Yb(8%):FOV under 0.3mw excitation, the absorption rate and the induced emission rate of $^4I_{15/2}$-$^4G_{11/2}$, when $^4G_{11/2}$ state is excited, are $1.5338\times10^{-4}\text{s}^{-1}$ and $1.9475\times10^{-6}\text{s}^{-1}$. The absorption rate and the induced emission rate of $^4I_{15/2}$-$^2H_{11/2}$, when $^2H_{11/2}$ state is excited, are $1.2026\times10^{-4}\text{s}^{-1}$

Table 1: The spontaneous emission rates of Er^{3+} ion in Er(1%)Yb(8%):FOV.

Initial level	Final level	Energy (cm^{-1})	A(s^{-1})
$^4I_{13/2}$	$^4I_{15/2}$	6410.3	190.99
$^4I_{11/2}$	$^4I_{15/2}$	9970.1	181.87
$^4I_{9/2}$	$^4I_{15/2}$	12165	99.634
$^4F_{9/2}$	$^4I_{15/2}$	14925	1401.6
$^4S_{3/2}$	$^4I_{13/2}$	11602	685.84
$^4S_{3/2}$	$^4I_{15/2}$	18182	1717.8
$^4F_{7/2}$	$^4I_{15/2}$	20202	3812.4
$^4F_{5/2}$	$^4I_{13/2}$	15384	1420.1
$^4F_{5/2}$	$^4I_{15/2}$	21964	2015.1
$^4F_{3/2}$	$^4I_{11/2}$	12212	1265.3
$^4F_{3/2}$	$^4I_{15/2}$	22450	1824
$(^2G^4F^2H)_{9/2}$	$^4I_{13/2}$	17769	1422.3
$(^2G^4F^2H)_{9/2}$	$^4I_{15/2}$	24349	1706.5
$^4G_{11/2}$	$^4I_{13/2}$	19578	1812.3
$^4G_{11/2}$	$^4I_{15/2}$	26157	12162
$^4G_{9/2}$	$^4I_{13/2}$	20626	7298.8
$^4G_{9/2}$	$^4I_{15/2}$	27206	2946.5

and $1.3267\times10^{-5}s^{-1}$. Other induced transition rates are much smaller because the large energy mismatch apart from the energy of pumping light.

Multi-phonon relaxation rate is related with the temperature and energy gap of the transition. Under certain temperature, the relationship between the rate and the energy gap can be expressed by exponential form as follow:

$$W_{mpr} = W_0 \exp(-\alpha \Delta E), \tag{3.2}$$

where W_0 is relaxation rate extrapolated to zero gap. If nonradiative processes are dominated by multi-phonon relaxation, the relationship among the relaxation rate, lifetime of energy level and spontaneous emission rate can be expressed as follow:

$$\sum W_{mpr} = \frac{1}{\tau} - \sum A. \tag{3.3}$$

The summation is over all of the terminal level. We measured the lifetime of Er^{3+} in the Er(0.5%):FOV, which reflect the environment of the host FOV and will be adopted in the calculation of Er(1%)Yb(8%):FOV. Thus considering the spontaneous emission rates obtained above, we can fit the two parameters W_0 and α. After that we can obtain the multi-phonon relaxation rates of every two levels according to Eq. (3.2). The main results are shown in Table 2.

In the rate equation (3.1), $W_p^{(m\to n,k\to i)}$ is the probability of energy transfer and back energy transfer processes, m and k denote the initial levels of two ions, and n and i stand

Table 2: The multi-phonon relaxation rates of Er^{3+} ion in Er(1%)Yb(8%):FOV.

Initial level	Final level	Energy (cm^{-1})	Wmpr(s^{-1})
$^4I_{13/2}$	$^4I_{15/2}$	6410.3	0.14261
$^4I_{11/2}$	$^4I_{13/2}$	3390.3	495.88
$^4I_{9/2}$	$^4I_{11/2}$	1926.9	25783
$^4F_{9/2}$	$^4I_{9/2}$	2441	6434.5
$^4S_{3/2}$	$^4F_{9/2}$	2882.9	1951.4
$^2H_{11/2}$	$^4S_{3/2}$	576.98	9.87e+05
$^4F_{7/2}$	$^2H_{11/2}$	1007.8	3.08e+05
$^4F_{5/2}$	$^4F_{7/2}$	1429.7	98716
$^4F_{3/2}$	$^4F_{5/2}$	225.03	2.55e+06
$(^2G^4F^2H)_{9/2}$	$^4F_{3/2}$	1698.6	47754
$^4G_{11/2}$	$(^2G^4F^2H)_{9/2}$	1499	81864
$^4G_{9/2}$	$^4G_{11/2}$	698.08	7.12e+05
$^4K_{15/2}$	$^4G_{9/2}$	358.69	1.78e+06

for the final levels. The energy transfer rate can be obtained by using the theories of Kushida, Dexter and Miyakawa [11, 12].

Kushida has expressed the expansion of electrostatic interaction Hamiltonian as tensor operator form. Using the Judd-Ofelt theory of rare earth electric dipole transition, he obtained the transfer rate expressions of dipole-dipole, dipole-quadrupole, quadrupole-dipole and quadrupole-quadrupole interaction [3]. Thus we can obtain the energy transfer rates without energy mismatch by the intensity parameters we have calculated above. But phonon-assisted energy transfer usually plays a much more general action. Miyakawa and Dexter proposed that the relationship between the energy transfer probability and the energy mismatch compensated by phonons is similar to the relationship of multi-phonon relaxation, which can be expressed as:

$$W_{PET}(\Delta E) = W_{PET}(0)\exp(-\beta\Delta E), \tag{3.4}$$

where ΔE is the energy mismatch, β is a parameter determined by electron-phonon coupling strength and properties of phonons that participate in the energy transfer: $\beta = \alpha - (1/\hbar\omega)\cdot\ln(1+g_D/g_A)$, where g is electron-phonon coupling constant and $\hbar\omega$ is the energy of phonons which play a major role in the energy transfer. Since the value of g does not change much, we assume that $g_D = g_A = g$ during the calculation [10]. The value of α has been fit when we calculated the multi-phonon relaxation rate. Thus all of the parameters in the rate equation (3.1) are achieved. Some rates of key energy transfer processes are listed in Table 3.

During the calculation, 15 coupled differential equations, of which the forms are same as Eq. (3.1) are solved by numerical iterative method. Two of them describe Yb^{3+} ions, and the others of them describe Er^{3+} ions (from the ground level $^4I_{15/2}$ to the excited level $^2K_{15/2}$). If dt is small enough, $n(t+\Delta t) = n(t) + \Delta t\cdot dn/dt$ is tenable, where we set it

Table 3: The key energy transfer rates between Er^{3+} ion and Yb^{3+} ion in Er(1%)Yb(8%): FOV.

Er^{3+}							W_{PET} $\times N_{Er}$ $\times N_{Yb}$	W_{PET}-im $\times N_{Er}$-im $\times N_{Yb}$-im
Initial level	Final level	Energy (cm^{-1})	W_{PET} (s^{-1})	W_{PET}-im (s^{-1})	N_{Er}	N_{Er}-im	(s^{-1})	(s^{-1})
$^4G_{11/2}$	$^4F_{9/2}$	478.5	7.15e+06	7.15e+06	2.12e-11	2.12e-11	1.52e-04	1.52e-04
$^4I_{15/2}$	$^4I_{11/2}$	-297.6	5.29e+05	1.27e+05	1	1	3.99e-01	1.83e-02
$^4F_{7/2}$	$^4G_{9/2}$	2637.2	9.83e+04	9.83e+04	8.98e-13	2.98e-12	6.66e-14	4.22e-14
$^4I_{11/2}$	$^4S_{3/2}$	716.9	2.24e+05	2.24e+05	5.96e-07	1.95e-07	1.01e-07	6.29e-09
$^4I_{9/2}$	$^4F_{5/2}$	-118.7	4.90e+05	2.77e+05	6.15e-09	4.48e-09	2.28e-09	1.79e-10
$^4F_{9/2}$	$(^2G^4F^2H)_{9/2}$	207.9	2.76e+05	2.76e+05	1.12e-08	1.87e-08	2.33e-09	7.43e-10
$^4S_{3/2}$	$^4G_{9/2}$	617	3.52e+04	3.52e+04	2.17e-10	2.86e-11	5.77e-12	1.45e-13
$^4S_{3/2}$	$^2K_{15/2}$	-41.3	5.05e+03	4.14e+03	2.17e-10	2.86e-11	8.27e-13	1.71e-14
$^4I_{15/2}$	$^2K_{15/2}$	-18223	2.14e-05	2.37e-43	1	1	1.62e-11	3.41e-50
$^4I_{15/2}$	$^4G_{9/2}$	-17565	6.74e-06	1.75e-42	1	1	5.09e-12	2.52e-49
$^4I_{15/2}$	$^4G_{11/2}$	-16567	5.00e-03	1.54e-37	1	1	3.78e-09	2.22e-44

The column of W_{PET} lists the phonon-assisted energy transfer rates calculated by the original theory. The column of W_{PET}-im lists the phonon-assisted energy transfer rates calculated by our improved theory which is introduced $\exp(hc\tilde{v}_k/kT)$ factor. The real transfer rates are the products of W_{PET}(-im) and the population probabilities of two ions' initial levels. The columns of N_{Er} and N_{Er}-im, which correspond to the results calculated by original theory and improved theory respectively, list the population probabilities of corresponding Er ions' initial levels when the sample is excited by 378nm-0.3mw light and fluorescence system gets stable. Relatively, the population probabilities of Yb ions' excited level $^2F_{5/2}$ are 7.55e-07 (N_{Yb}) and 1.44e-07 (N_{Yb}-im), which correspond to the results calculated by original theory and improved theory respectively and when the sample is excited by 378nm-0.3mw light. Under weak excitation, the population probabilities of Er and Yb ions' ground levels are always nearly equal to 1. And the last two columns are the results of real transfer rates whether we consider the introduced factor or not. The first energy transfer in line 1 is a forward energy transfer from Er^{3+} to Yb^{3+}, the Yb^{3+} ion is excited from the ground state $^2F_{7/2}$ to the excited state $^2F_{5/2}$. The other transfers are back energy transfers from Yb^{3+} to Er^{3+} and the initial level of Yb^{3+} ion is the excited state $^2F_{5/2}$.

to 5×10^{-10}s in the calculation. Considering that the initial conditions of the population probabilities are 1 for the ground level and 0 for the excited levels, as well as the real transition rates are the products of the rates listed in Table 3 and the population probabilities of transition initial levels at the previous moment, we will obtain the curves of each level's population probabilities *vs* time, and after being stabilized the data will finally be taken as the solution of the equations.

4 Discussion on Stokes and anti-Stokes energy transfer

Following the classification of Bron and Wagner [11], triply ionized rare earth ions in usual matrices for laser or summation of photon action by energy transfer appear to fall

in the class that small change in mass and spring constants and weak election-lattice coupling. Using the Kubo-Toyozawa-Lax generating function method, adiabatic approximation and linear coupling, in the case of small-g coupling constant (low temperature with respect to maximum phonon energy of the lattice), Miyakawa and Dexter have obtain expression of energy transfer probability [4]

$$W_{ab}=(2\pi/\hbar)|H_{ab}|^2\sum_N e^{-(g_a+g_b)}(g_a+g_b)^N/N!\sigma_{ab}\delta(\varepsilon_0-N\hbar\omega), \tag{4.1}$$

where g_a and g_b are the electron-phonon coupling functions of energy donor and accepter related to S_0, the Pekar-Huang-Rhys coupling constant by $g=S_0(2\overline{n})+1$, n being the occupation number for the effective phonons of energy $\hbar\omega$ where ω is assumed to be maximum lattice frequency. σ_{ab} is the overlap integral between ions a and b for zero-order process. Considering the N-phonon process taken as $N=\Delta E/\hbar\omega$, if we set $g_a+g_b=r$, the Eq. (4.1) can be written as:

$$W_{ab}=(2\pi/\hbar)|H_{ab}|^2\sigma_{ab}\cdot e^{-r}r^N/N!. \tag{4.2}$$

Note that the form of the part $e^{-r}r^N/N!$ is the same as the form of "Pekarian" lineshape at 0°K which resembles a double Gaussian [12]. According to the [12], at finite temperature in the phonon-assisted energy transfer processes in which phonons are emitted, $e^{-r}r^N/N!$ can be replaced by $e^{-r}r^N/N!F_N(T,r)$ with

$$F_N(T,r)=e^{-2r\overline{n}}\sum_{l=0}^{\infty}\frac{N!}{l!(l+N)!}(1+\overline{n})^{l+N}(\overline{n}r^2)^l. \tag{4.3}$$

For small $\overline{n}$, r and large N, Eq. (4.3) reduces to $(\overline{n}+1)^N$. We suppose $g=S_0$ [13, 14] and associate with , $g_a+g_b=r$ as a result, for phonon-assisted energy transfer processes, assuming that phonons are mainly emitted, the expression of probability can be written as:

$$W_{Stokes-ab}(N)=(2\pi/\hbar)|H_{ab}|^2\sigma_{ab}\frac{e^{-(S_{0a}+S_{0b})}(S_{0a}+S_{0b})^N}{N!}(1+\overline{n})^N. \tag{4.4}$$

For anti-Stokes phonon-assisted energy transfer, where the transferred energy is less than the accepted energy and phonons are mainly absorbed, we have equivalently

$$W_{anti-Stokes-ab}(N)=(2\pi/\hbar)|H_{ab}|^2\sigma_{ab}\frac{e^{-(S_{0a}+S_{0b})}(S_{0a}+S_{0b})^N}{N!}(\overline{n})^N \tag{4.5}$$

with $\overline{n}=(e^{\hbar\omega/kT}-1)^{-1}$. By using the Stirling's approximation for $N!\approx(N/e)^N$ and energy mismatch $\Delta E=N\hbar\omega$, Eqs. (4.4) and (4.5) are written as

$$W_{Stokes-ab}(N)=(2\pi/\hbar)|H_{ab}|^2\sigma_{ab}e^{-(S_{0a}+S_{0b})}e^{-\beta\Delta E}, \tag{4.6}$$

$$W_{anti-Stokes-ab}(N)=(2\pi/\hbar)|H_{ab}|^2\sigma_{ab}e^{-(S_{0a}+S_{0b})}e^{-(\beta+1/kT)\Delta E}, \tag{4.7}$$

with β defined as

$$\beta=(\hbar\omega)^{-1}\left(\ln\left(\frac{N}{S_{0a}(\overline{n}+1)}\right)-\ln\left(1+\frac{S_{0b}}{S_{0a}}\right)-1\right).$$

Consider the definition of α in the multi-phonon relaxation processes,

$$\beta=\alpha-(\hbar\omega)^{-1}\ln\left(1+\frac{S_{0b}}{S_{0a}}\right)$$

which is the same as the expression in [4], but with $g=S_0$.

Note that the expressions of phonon-assisted energy transfer for Stokes process and anti-Stokes process are nearly same, but different with a factor $\exp\{\Delta E/kT\}$ which is the ratio between the $W_{Stokes-ab}$ and $W_{anti-Stokes-ab}$. As we know, it is the first time by us to express this difference between the Stokes process and anti-Stokes process in the energy transfer theory apparently like Eqs. (4.6) and (4.7). Obviously, we should pay much attention to this difference just like similar phenomenon in the Raman scattering theory.

In classical Raman theory the intensity ratio between the Stokes process and anti-Stokes process can be expressed as $(\omega_L-\omega_q)^4/(\omega_L+\omega_q)^4$. However, this classical Raman theory can not well explain the experimental intensity ratio between the Stokes and anti-Stokes Raman signal. As we known, the intensity of Raman scattering in quantum theory [15] can be expressed by:

$$I_{Stokes}=const\cdot\left(\omega_L-\omega_q\right)^4\frac{\hbar}{2\omega_q}\alpha^2_{\beta\varphi,q}\left(1+\overline{n_q}\right), \tag{4.8}$$

$$I_{anti-Stokes}=const\cdot\left(\omega_L+\omega_q\right)^4\frac{\hbar}{2\omega_q}\alpha^2_{\beta\varphi,q}\overline{n_q}, \tag{4.9}$$

where $\overline{n_q}$ is the average population probability of a certain elementary excitation which is phonon here and satisfies the Bose-Einstein distribution

$$\overline{n_q}=[\exp(\hbar\omega_q/k_BT)-1]^{-1}.$$

Substituting this into Eqs. (4.8) and (4.9), there is an additional coefficient

$$(1+\overline{n_q})/\overline{n_q}=\exp(\hbar\omega_q/k_BT)$$

for the ratio of I_{Stokes} and $I_{anti-Stokes}$ in quantum Raman theory compared with classical Raman theory. Thus, the experimental phenomenon of Raman spectroscopy is well explained by quantum Raman theory quantitatively. It is this very coefficient that makes the trouble in the relationship between the Stokes and anti-Stokes process intensities in the classical Raman theory solvable. Note that this coefficient is same as what we obtained in the energy transfer theory. And it comes from the differences among the transitions of vibrational levels. In general, most of the molecules are in the ground vibrational state,

with very few situated at high vibrational states. Therefore the vibrational transitions that start from the ground vibrational level have much larger probabilities, which correspond to the Stokes processes where the electronic system loses energy to the vibrational system. These discussions are suitable as well to the phonon-assisted energy transfer processes involving energy exchange between the electronic system and vibrational system. Therefore the difference between energy absorption and energy radiation in the vibrational system must be reflected in the phonon-assisted energy transfer like Eqs. (4.6) and (4.7).

Similar result was also achieved by Auzel in discussing the Stokes and anti-Stokes phonon sideband excitation fluorescence [12]. Take $g=S_0$ and with "Pekarian" forms at 0°K ($e^{-S_0}S_0^N/n!$) in the processes, and consider small $\overline{n}$, S_0 and large N, the order of the multiphonon process involved, the probability for multiphonon Stokes and anti-Stokes excitation can be expressed as follows by using Stirling's developments:

$$W_{Stokes}(\Delta E)=\frac{I}{c}\frac{8\pi^3}{3h^2}|M|^2e^{-S_0}e^{-\alpha_S\Delta E}, \tag{4.10}$$

$$W_{anti-Stokes}(\Delta E)=\frac{I}{c}\frac{8\pi^3}{3h^2}|M|^2e^{-S_0}e^{-(\alpha_S+1/kT)\Delta E}, \tag{4.11}$$

where $\alpha_S=(\hbar\omega_m)^{-1}\{\ln[N/S_0(\overline{n}+1)]-1\}$ and $\hbar\omega_m$ is the effective phonon energy. We can find that there is a factor $\exp\{\Delta E/kT\}$ either between Stokes process and anti-Stokes process, where ΔE is the energy gap between the excitation and the electronic level. These results are coincident with what we have supposed that the difference between the Stokes process and anti-Stokes process should possess the same form in the system which involves energy exchange between the electronic system and vibrational system.

Using tensor operator to expend electronic coulomb interaction between the donor and accepter and following the statements of Judd-Ofelt theory, Kushida have obtained the rates of resonance energy transfer as follows [3]:

$$W_{ab}^{(d-d)}=\frac{1}{(2J_a+1)(2J_b+1)}\left(\frac{2}{3}\right)\left(\frac{2\pi}{\hbar}\right)\left(\frac{e^2}{R^3}\right)^2 \times\left[\sum_\lambda\Omega_{A\lambda}\left\langle J_a\middle\|U^{(\lambda)}\middle\|J_a'\right\rangle\right]\left[\sum_\lambda\Omega_{B\lambda}\left\langle J_b\middle\|U^{(\lambda)}\middle\|J_b'\right\rangle\right]S, \tag{4.12}$$

$$W_{ab}^{(d-q)}=\frac{1}{(2J_a+1)(2J_b+1)}\left(\frac{2\pi}{\hbar}\right)\left(\frac{e^2}{R^4}\right)^2 \times\left[\sum_\lambda\Omega_{A\lambda}\left\langle J_a\middle\|U^{(\lambda)}\middle\|J_a'\right\rangle\right]\langle 4f|r_B^2|4f\rangle^2\left\langle f\middle|C^{(2)}\middle|f\right\rangle^2\left\langle J_b\middle\|U^{(2)}\middle\|J_b'\right\rangle^2S, \tag{4.13}$$

$$W_{ab}^{(q-q)}=\frac{1}{(2J_a+1)(2J_b+1)}\left(\frac{14}{5}\right)\left(\frac{2\pi}{\hbar}\right)\left(\frac{e^2}{R^5}\right)^2 \times\langle 4f|r_A^2|4f\rangle^2\langle 4f|r_B^2|4f\rangle^2\left\langle f\middle|C^{(2)}\middle|f\right\rangle^2\left\langle J_a\middle\|U^{(2)}\middle\|J_a'\right\rangle\left\langle J_b\middle\|U^{(2)}\middle\|J_b'\right\rangle^2S, \tag{4.14}$$

where $d-d$, $d-q$ and $q-q$ represent the dipole-dipole, dipole-quadrupole and quadrupole-quadrupole interaction between the ions, Ω_λ ($\lambda = 2,4,6$) is the Judd-Ofelt intensity parameters, R is the ions' distance between the energy donor and acceptor, S is the overlap integral of the donor's emission spectrum and acceptor's absorption spectrum. And $\langle J_a \| U^{(\lambda)} \| J'_a \rangle$ is the reduced matrix element of the unit tensor operator U between the two states of the ion. When energy mismatch exists between the donor and acceptor ions, the energy transfer can occur accompanied by the emission or absorption of phonons. For the rate of such a phonon-assisted energy transfer, Eq. (3.4) by Miyakawa and Dexter was theoretically proposed with $W_{PET}(0)$ denotes the transfer rate for the energy matched case. But these formulas which we use in the calculation do not involve the difference between the Stokes process and anti-Stokes process. In present paper we process the energy transfer theory on this point further. Thus the coefficient $\exp(hc\widetilde{v}_k/kT)$ was introduced to improve the calculation of energy transfer rate described by the original theory [3, 4]. The original Kushida theory is tenable and unchanged. The original phonon-assistant Miyakawa and Dexter theory (Eq. (3.4)) is considered reasonable only for discussing Stokes processes, whereas the rate of anti-Stokes energy transfer should be divided by the introduced coefficient $\exp(hc\widetilde{v}_k/kT)$, where $\widetilde{v}_k$ is the mismatch of energy transfer. Table 3 lists some improved rates of energy transfer. After this introduction, some anti-Stokes energy transfer rates, which involve the ground level of Er^{3+} ion as initial level such as

$$\{^2F_{5/2}(Yb^{3+}) \longrightarrow {}^2F_{7/2}(Yb^{3+}),\ {}^4I_{15/2}(Er^{3+}) \longrightarrow {}^4G_{11/2}(Er^{3+})\},$$
$$\{^2F_{5/2}(Yb^{3+}) \longrightarrow {}^2F_{7/2}(Yb^{3+}),\ {}^4I_{15/2}(Er^{3+}) \longrightarrow {}^4G_{9/2}(Er^{3+})\},$$
$$\{^2F_{5/2}(Yb^{3+}) \longrightarrow {}^2F_{7/2}(Yb^{3+}),\ {}^4I_{15/2}(Er^{3+}) \longrightarrow {}^2K_{15/2}(Er^{3+})\},$$

reduce obviously as shown in Table 3. Note that the original energy transfer rates W_{PET} of these three channels, which are listed in 4^{th} column of Table 3, are indeed smaller than other channels which possess much smaller energy mismatch. But during the simulation, the real energy transfer rates is $W_{PET} \times N_{Er} \times N_{Yb}$, which includes the product with population probabilities of ions' initial levels. Through the 8^{th} column of Table 3 we find that these real transfer rates of above three transfer channels, which origin from one ion's ground state and possess very large energy mismatch, are too fast compared with other channels. It seems impossible for an anti-Stokes energy transfer channel whose mismatch is more than 15000cm^{-1} to absorb enough energy through the phonons to compensate the big gap. Thus the improved rates W_{PET}-im are more reasonable. These anti-Stokes energy transfer channels should have much lower transfer rates as shown in the last column in Table 3.

5 Simulation results

In order to discuss the importance of $\exp(hc\widetilde{v}_k/kT)$, let's take the range of intensity inversion Σ as example. Fig. 4 shows the simulation results with and without consider-

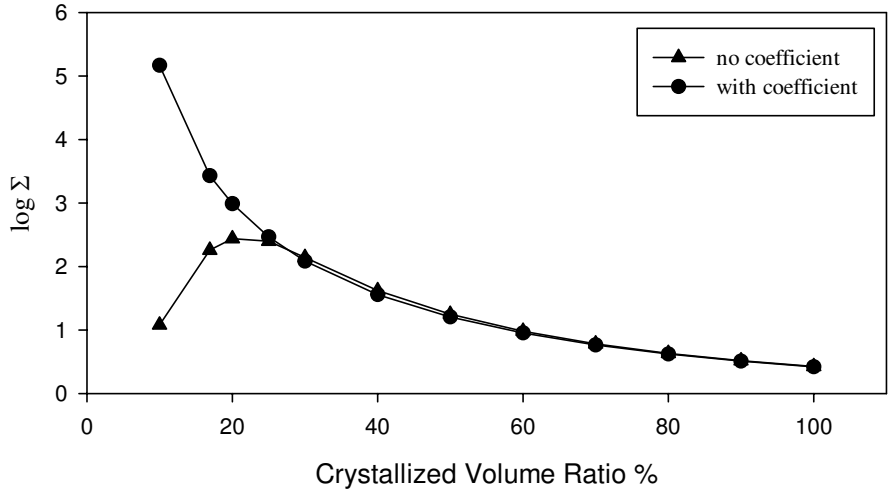

Figure 4: The range of intensity reversion Σ changes with the total crystallized volume ratio.

ing this coefficient using the logarithm of the Σ as the ordinate. In the simulation of Er(1%)Yb(8%): FOV, we suppose that all of the rare earth ions are incorporated into a nanocrystalline phase. If the total ion number of rare earth ion is fixed value, the small crystallized volume ratio of the FOV means the small distance between the rare earth ions. During the calculation, we change the total crystallized volume ratio from 10% to 100% with other parameter unchanged by setting different volumes of each rare earth ion in proportion. That is to say we simulate the system in different ions distance which changes from small to large.

The circles are the results considering the coefficient, while the triangles are those without taking the coefficient into account. The significant difference between the two lines lies in the range less than 25%, which is just in the range of most reported crystallized volume ratios in glass ceramics [16]. Note that the circle line is monotonically decreasing, whereas the triangle line is increasing firstly prior to decline. Obviously, the result without considering the coefficient deviates from the experiments and common sense. The values of Σ in samples doped with erbium at the same concentration and with ytterbium at different concentrations were studied experimentally [6]. The results imply that the Σ will decrease with the increase in the distance between ions and the concentration of ytterbium, which are in contradiction to the results shown by the triangle line but coincident with the circle line. In addition, as for the values of ordinates, the variation range in the circle line is larger, a result coincident with the experiment. But we can not even find a proper crystallized volume ratio for the triangle line to reflect the significant intensity inversion phenomenon because of its such a small value of Σ.

Consequently, for this phenomenon with energy transfer playing an important role, it is critical to introduce the coefficient to describe the difference between the Stokes and anti-Stokes energy transfer. Through the numerical simulation we found that when the

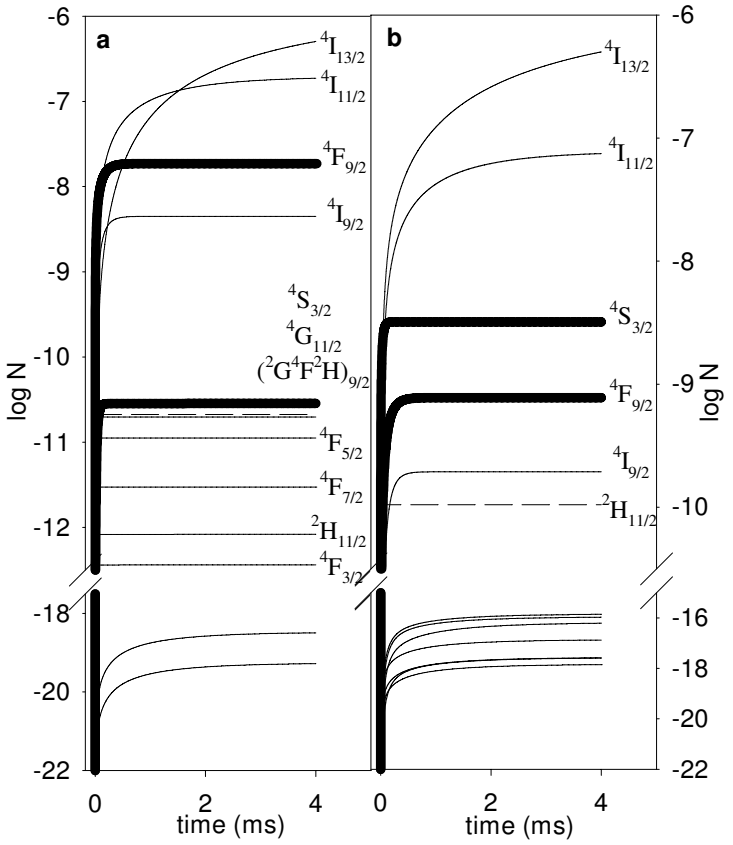

Figure 5: The simulation results of Er^{3+} level's population probabilities changing with time when Er(1%)Yb(8%):FOV is excited by 378.5nm light(a) and 522.3nm light(b). The total crystallized volume ratio in the glass ceramics is 16.9%.

total crystallized volume ratio is 16.9% the theoretical result of Σ is coincident with the experimental result perfectly. Considering the equation $I/N_i = n_i A_{ij} h\nu$ in general laser theory, when the simulated system has been stabilized, we can get that α is 6.16, γ is 437.73 and Σ is 2696.48. The calculation results of Er^{3+} level's population probabilities as a function of time are shown in Fig. 5, with the time as abscissa and the logarithm of the level's population probabilities as ordinate. Figs. 5a and 5b are the results when the material is excited by 378.5nm and 522.3nm light respectively. The numbers at the right of the curves represent the ordinal numbers of the excited levels from $^4I_{13/2}$ to $^2K_{15/2}$ of Er^{3+} ion. The curves of $^4F_{9/2}$ and $^4S_{3/2}$ are thick solid lines. The levels corresponding to the excitation energy, $^4G_{11/2}$ in Fig. 5a and $^2H_{11/2}$ in Fig. 5b, are showed by the dashed lines.

In Fig. 5a the population probability of $^4F_{9/2}$ is much higher than that of $^4S_{3/2}$. Considering the $I/N_i = n_i A_{ij} h\nu$, the red fluorescence is stronger than the green one, which is coincident with the experiment. When $^4G_{11/2}$ is excited directly, $^4F_{9/2}$ can be populated

rapidly through the energy transfer channel

$$\{^4G_{11/2}(Er^{3+}) \longrightarrow {}^4F_{9/2}(Er^{3+}), {}^2F_{7/2}(Yb^{3+}) \longrightarrow {}^2F_{5/2}(Yb^{3+})\}$$

because the fast transfer probability $W_p^{(m\to n,k\to i)}$ of this channel is up to 7.147×10^6. But there is not high speed transfer channel to $^4S_{3/2}$ whose population mainly comes from $^2H_{11/2}$ through multi-phonon relaxation. That is the reason why the population probability of $^4S_{3/2}$ is relatively lower than that of $^4F_{9/2}$. At the same time, the energy transfers from Er^{3+} to Yb^{3+} ions excite the Yb^{3+} ions from $^2F_{7/2}$ to $^2F_{5/2}$. The $^2F_{5/2}$ of Yb^{3+} is resonant with the $^4I_{11/2}$ of Er^{3+}. Consequently, another channel to populate $^4I_{11/2}$ of Er^{3+}, i.e.,

$$\{^2F_{5/2}(Yb^{3+}) \longrightarrow {}^2F_{7/2}(Yb^{3+}), {}^4I_{15/2}(Er^{3+}) \longrightarrow {}^4I_{11/2}(Er^{3+})\},$$

can be created with the rate of 1.269×10^5. Therefore, compared with Fig. 5b the curve of $^4I_{11/2}$ in Fig. 5a is raised much more quickly than the curve of $^4I_{13/2}$. The levels $^4G_{9/2}$ and $^2K_{15/2}$ are higher than $^4G_{11/2}$. Their population mainly come from the cooperative effects of back energy transfer channels such as

$$\{^2F_{5/2}(Yb^{3+}) \longrightarrow {}^2F_{7/2}(Yb^{3+}), {}^4I_{11/2}(Er^{3+}) \longrightarrow {}^4S_{3/2}(Er^{3+})\},$$
$$\{^2F_{5/2}(Yb^{3+}) \longrightarrow {}^2F_{7/2}(Yb^{3+}), {}^4I_{9/2}(Er^{3+}) \longrightarrow {}^4F_{5/2}(Er^{3+})\},$$
$$\{^2F_{5/2}(Yb^{3+}) \longrightarrow {}^2F_{7/2}(Yb^{3+}), {}^4F_{9/2}(Er^{3+}) \longrightarrow ({}^2G^4F^2H)_{9/2}(Er^{3+})\},$$
$$\{^2F_{5/2}(Yb^{3+}) \longrightarrow {}^2F_{7/2}(Yb^{3+}), {}^4F_{7/2}(Er^{3+}) \longrightarrow {}^4G_{9/2}(Er^{3+})\},$$
$$\{^2F_{5/2}(Yb^{3+}) \longrightarrow {}^2F_{7/2}(Yb^{3+}), {}^4S_{3/2}(Er^{3+}) \longrightarrow {}^4G_{9/2}(Er^{3+})\},$$
$$\{^2F_{5/2}(Yb^{3+}) \longrightarrow {}^2F_{7/2}(Yb^{3+}), {}^4S_{3/2}(Er^{3+}) \longrightarrow {}^2K_{15/2}(Er^{3+})\}.$$

Because the population probability products of the excited Yb^{3+} and Er^{3+} initial levels in these energy transfers are much lower, the higher levels $^4G_{9/2}$ and $^2K_{15/2}$ have little population probability. The same situations for $^4F_{7/2}$ to $^4G_{9/2}$ occur in Fig. 5b too, where it is obvious that there is no intensity inversion phenomenon. Because $^2H_{11/2}$ is excited directly, the population probability of $^4G_{11/2}$ is very low and the channel

$$\{^4G_{11/2}(Er^{3+}) \longrightarrow {}^4F_{9/2}(Er^{3+}), {}^2F_{7/2}(Yb^{3+}) \longrightarrow {}^2F_{5/2}(Yb^{3+})\}$$

has no effect. The population probabilities of $^4S_{3/2}$ and $^4F_{9/2}$ mainly come from the multi-phonon relaxation. That's why in Fig. 5b from the curve of $^2H_{11/2}$ to $^4I_{13/2}$, we see that the higher levels become stabilized a little more quickly than the next lower levels.

6 Conclusion

In the present study we integrate every theory about the fluorescence process including induced emission, absorption, spontaneous emission, multi-phonon relaxation, and

energy transfer to numerically simulate an interesting photonic phenomenon the fluorescence intensity inversion between red and green fluorescence of Er(1%)Yb(8%):FOV nanophase oxyfluoride vitroceramics. Especially we place stress on the introduction of an extra coefficient $\exp(hc\widetilde{v}_k/kT)$ to original energy transfer theory based on Auzel's discussion. The coefficient reflects the difference between the Stokes process and anti-Stokes process. By using the improved theory we obtain the simulation results which are coincident with the experiment results perfectly. And through comparing the results with and without considering this coefficient, we found that it is essential to take the coefficient into calculation particularly for the nano-materials where energy transfer plays a key role.

Acknowledgments

The research was supported by the National Natural Science Foundation of China (10674019). The authors would like to thank Prof. Francois Auzel at France, Prof. Bingkun Zhou at Tsinghua University and Prof. Fanglin Peng at Beijing Normal University for useful guidance.

References

[1] F. Auzel, Upconversion and anti-Stokes processes with f and d ions in solids, Chem. Rev. 104 (2004), 139-173.
[2] B. Simondi-Teisseire, B.Viana, D.Vivien, A.M.Lejus, Yb^{3+} to Er^{3+} energy transfer and rate-equations formalism in the eye safe laser material Yb:Er:$Ca_2Al_2SiO_7$, Opt. Mater. 6 (1996), 267-274.
[3] T. Kushida, Energy transfer and cooperative optical transitions in rare-earth doped inorganic materials. I. Transition probability calculation, J. Phys. Soc. Japan 34 (1973), 1318-1326.
[4] T. Miyakawa and D. L. Dexter, Phonon sidebands, multiphonon relaxation of excited states, and phonon assisted energy transfer between ions in solids, Phys. Rev. B 1 (1970), 2961-2969.
[5] B. Henderson, G. F. Imbusch, Optical Spectroscopy of Inorgannic Solids (Clarendon Press, Oxford, 1989).
[6] X. B. Chen, Z. F. Song, L. L. Hu, J. J. Zhang and L. Wen, Experimental study on a nonlinear photonics process of Er(0.5)Yb(3):FOV oxyfluoride nanophase vitroceramics, Opt. Lett. 32 (2007), 2019-2021.
[7] W. T. Carnell, P. R. Fields and B. G. Wybourne, Spectral intensities of the trivalent lanthanides and actinides in solution. I. Pr^{3+}, Nd^{3+}, Er^{3+}, Tm^{3+}, and Yb^{3+}, J. Chem. Phys. 42 (1965), 3797-3806.
[8] A. A. Kaminskii, Laser Crystals (New York: Springer-Verlag, 1981).
[9] M. J. Weber, Probabilities for Radiative and Nonradiative Decay of Er^{3+} in LaF_3, Phys. Rev. 157 (1967), 262-272.
[10] J. L. Kennedy and N. Djeu, Energy transfer in rare earth doped $Y_3Al_5O_{12}$ at very high temperature, J. Lumin. 101 (2003), 147-153.
[11] W. E. Bron and M. Wagner, Rare-earth ions in the alkali halides. III. Electron-lattice coupling and the details of the vibronic spectra, Phys. Rev. 139 (1965), A223-A241.

[12] M. D. Sturge, Temperature dependence of multiphonon nonradiative decay at an isolated impurity center, Phys. Rev. B 8 (1973), 6-14.
[13] L. A. Riseberg and H. W. Moos, Multiphonon orbit-lattice relaxation of excited states of rare-earth ions in crystals, Phys. Rev. 174 (1968), 429-438.
[14] F. Auzel, Multiphonon-assisted anti-Stokes and Stokes fluorescence of triply ionized rare-earth ions, Phys. Rev. B 13 (1976), 2809-2817.
[15] D. A. Long, Raman Spectroscopy (McGraw-Hill, New York, 1977).
[16] M. Beggiora, I. M. Reaney, M. S. Islam, Structure of the nanocrystals in oxyfluoride glass ceramics, Appl. Phys. Lett. 83 (2003), 467-469.